Available online at www.sciencedirect.com
ScienceDirect
Acta Materialia 57 (2009) 932–939
Acta MATERIALIA
www.elsevier.com/locate/actamat

Micro-truss nanocrystalline Ni hybrids

L.M. Gordon [a], B.A. Bouwhuis [a], M. Suralvo [a], J.L. McCrea [b], G. Palumbo [b], G.D. Hibbard [a,*]

[a] Department of Materials Science and Engineering, University of Toronto, Room 140, 184 College Street, Toronto, Ont., Canada M5S 3E4
[b] Integran Technologies Inc., 1 Meridian Road, Toronto, Ont., Canada

Received 27 August 2008; accepted 23 October 2008
Available online 25 November 2008

Abstract

A low-density nanocrystalline material was created by electroforming nanocrystalline Ni around a rapid prototyped acrylic photopolymer micro-truss. This new hybrid material combines the structural efficiency of micro-truss architectures with the ultra-high strength that can be achieved by grain size reduction to the nanometer scale. A range of strut thicknesses were electrodeposited and tested in uniaxial compression. Strut failure occurred by inelastic buckling in the core (compression) members and tensile fracture in the face-sheet (tension) members. Experimental knockdown factors were determined from the idealized compressive modulus and peak strength models and used to map the optimal strut geometry in terms of deposited Ni and the initial strut cross-section.

Keywords: Cellular materials; Nanocrystalline materials; Nickel; Buckling; Electroplating

1. Introduction

The strength increase associated with grain size reduction to the nanometer scale has driven extensive research efforts in the development of nanocrystalline materials (e.g., reviews in [1–5]). A significant issue from early studies was the effect of synthesis limitations on both the quantity and quality of nanocrystalline materials that could be produced (e.g. [1,2]). The majority of early mechanical property measurements were made by hardness measurements because of the difficulties in making enough material to produce tensile coupons [1,2]. When tensile coupons could be made, they were often sub-sized and typically exhibited poor ductility. For example, early tensile tests of nanocrystalline materials produced by electrodeposition reported large yield strength increases but poor elongations to fracture (often below 1%) (e.g. [6,7]). In addition, size effects had been reported in which lower fracture strengths were measured in larger tensile coupons [8,9]. Such issues were likely the result of processing flaws, e.g., hydrogen pit holes and co-deposited bath impurity particulate, introduced during electrodeposition in small-scale plating systems [10]. With improvements in electrosynthesis methods in pilot plant and full production environments, much higher ductility values have been obtained, and electrodeposition has emerged as a technologically and economically viable route to produce nanocrystalline metals and alloys [11]. For example, a recent study has shown that the electrosynthesis method can be scaled up to produce relatively large-scale nanocrystalline Ni alloy electroforms (>2 mm thickness) exhibiting tensile elongations to failure in excess of 10% without any deleterious size effects [12].

Nonetheless, for many potential structural applications the density of a nanocrystalline material is just as important as its strength. In fact, reducing the density is more important than increasing the strength for certain weight specific materials performance indices (e.g. [13]). One way to reduce the density of a nanocrystalline material is to incorporate an internal void structure, i.e., creating a hybrid of nanocrystalline metal and space. Metal foams have been widely investigated and are broadly classified on the basis of the connectivity of the porosity; open-cell foam architectures can allow multi-functional applications, such as thermal exchange, energy absorption and catalytic support [14]. However, metal foams have bending-domi-

* Corresponding author. Tel.: +1 416 946 0437; fax: +1 416 978 4155.
E-mail address: glenn.hibbard@utoronto.ca (G.D. Hibbard).

1359-6454/$34.00
doi:10.1016/j.actamat.2008.10.038

nated cellular architectures, meaning that externally applied loads are generally resolved transversely to the ligaments or webs that make up the cellular architecture [14,15]. In contrast, the architecture of cellular micro-truss materials are specifically designed such that the internal struts are loaded in compression or tension; the stretch-dominated loading characteristics of micro-trusses can be substantially more efficient than the bending-dominated behaviour of conventional metal foams [15]. Nanocrystalline micro-trusses represent a new class of nanocrystalline materials that combine the most efficient cellular architectures with the high strength that comes from nanometer scale grain sizes, allowing new regions of material property space to be accessed.

Electrodeposition is particularly suited to the development of nanocrystalline micro-truss materials since virtually any cathode geometry can be used as a starting template. Recently we have reported on a hybrid nanocrystalline cellular material in which high-strength nanocrystalline Ni–Fe sleeves were electroformed around an aluminum alloy micro-truss [16]. The cathode template in that initial study was fabricated by stretch-bending a perforated aluminum sheet into a three-dimensional pyramidal architecture. The load-bearing capacity of the electroformed composite struts was shared between the aluminum core and the nanocrystalline sleeve; sleeve thicknesses ranged from 75 to 400 μm and had the effect of increasing the inelastic buckling strength of the aluminum struts by up to a factor of 12 [16]. The present study takes a different approach, creating a nanocrystalline metal/polymer hybrid cellular material by first fabricating a low-density polymer micro-truss through rapid prototyping. This is a compelling approach since a much broader range of micro-truss architectures can be fabricated by rapid prototyping than can be achieved by the stretch-bending plastic deformation method used in our previous study.

2. Experimental

Pyramidal micro-truss pre-forms were obtained from FineLine Prototyping (of Raleigh, NC). The micro-trusses were fabricated by rapid prototyping using a proprietary acrylic photopolymer on a InVision HR 3-D Modeler (3D Systems Inc., Rock Hill, SC). A rendering of the computer-aided design model used to fabricate the pre-forms is shown in Fig. 1 (sample size 17.8 mm × 17.8 mm × 1.5 mm). The truss angle was $\omega = 45°$ and the truss core strut lengths, thicknesses and widths were $l = 1.38$ mm, $a = 0.18$ mm and $b = 0.39$ mm, respectively. The mass of the starting pre-form was $m_{\text{polymer}} = 66.2$ mg and the starting micro-truss density was $\rho = 0.046\ \text{Mg m}^{-3}$ (corresponding to a relative density of 4.5%). The acrylic photopolymer was assumed to follow an elastic/perfectly plastic constitutive behaviour, with a modulus of 1.7 GPa and a yield strength of 32 MPa [17].

The as-received polymer cores were metallized using standard methods and nanocrystalline Ni was pulse current

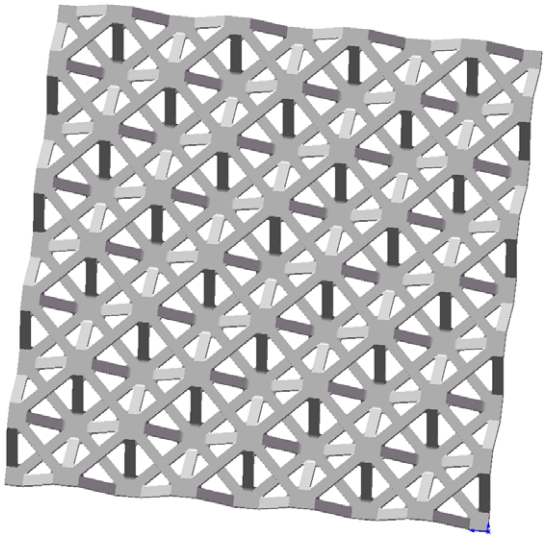

Fig. 1. Rendering of the model used for rapid prototyping the micro-truss polymer core.

electrodeposited, after Refs. [18,19]. Fig. 2 presents a scanning electron microscopy (SEM) image of an as-deposited micro-truss. The nanostructure of the Ni was characterized by X-ray diffraction (XRD) using Co Kα radiation ($\lambda = 0.179$ nm). Fig. 3 presents a typical XRD pattern along with a reference pattern for a Ni powder standard. An average grain size of 22 nm was measured from the diffraction peak broadening, which is typical of nanocrystalline Ni produced by pulse current electrodeposition (e.g. [20,21]). A reference tensile curve for nanocrystalline Ni deposited using the same conditions and having the same as-deposited grain size (yield strength of $\sigma_{\text{YS}} = 780$ MPa) [22] was fit to a sixth-order polynomial and used for the

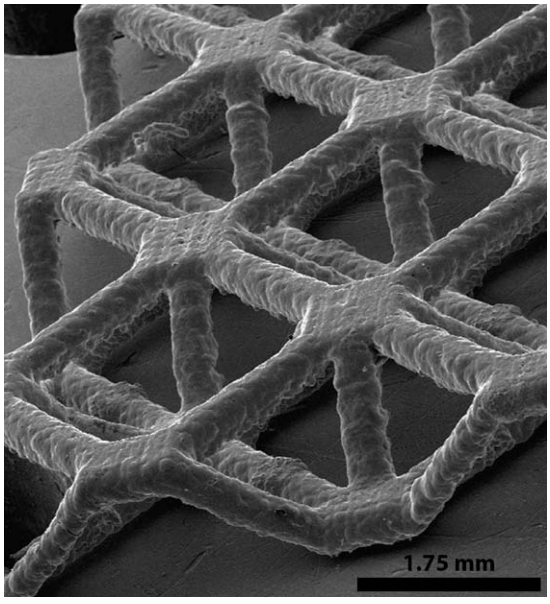

Fig. 2. SEM micrograph of an as-deposited nanocrystalline Ni micro-truss.

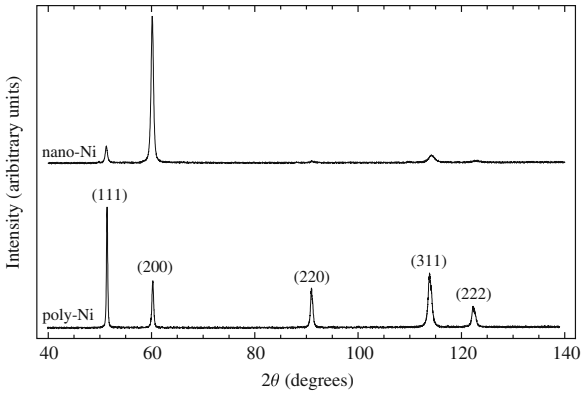

Fig. 3. XRD pattern ($\lambda = 0.179$ nm) for electrodeposited nanocrystalline Ni and a polycrystalline nickel standard.

inelastic buckling analysis. Note that the reference tensile elastic modulus (150 GPa) was lower than Young's modulus for conventional polycrystalline Ni (207 GPa [23]) and may be related to crystallographic texture effects in the electrodeposit. A nominal thickness for the electrodeposited nickel was calculated based on the increase in mass during the plating process by assuming a uniform thickness of nickel over the entire surface area of the micro-truss. The nominal nanocrystalline Ni sleeve thicknesses t_{Ni} ranged from 15.1 ± 0.5 to 56.7 ± 1.4 μm, and are summarized in Table 1. The area fraction of Ni f_{Ni} in the strut cross-sections was determined from the relationship:

$$f_{Ni} = \frac{2t_{Ni}(a + b + 2t_{Ni})}{ab + 2t_{Ni}(a + b + 2t_{Ni})} \quad (1)$$

The nominal Ni strut fractions ranged from 0.21 to 0.53 (Table 1) and the micro-truss densities ranged from ~1.5% to 5% of the density of bulk nanocrystalline Ni.

Mechanical properties of the as-received acrylic photopolymer micro-trusses and the electrodeposited nanocrystalline Ni micro-trusses were evaluated in uniaxial compression. Samples were compressed at a loading rate of $2 \times 10^{-3}\ s^{-1}$ using a Shimadzu AG-50kN-I (Kyoto, Japan) load frame. Recorded displacements, adjusted for machine compliance based on the measured load, were used to estimate the compressive strain. Failure mechanisms in the electroformed micro-truss were investigated by SEM characterization of samples pre-loaded to strains of approximately 0.10, 0.18 and 0.25.

Table 1
Mechanical properties of the as-received rapid prototyped micro-trusses and electrodeposited nanocrystalline Ni micro-trusses summarizing the nominal nanocrystalline Ni sleeve thickness (t_{Ni}), fraction Ni in strut cross-section (f_{Ni}), density (ρ), elastic modulus (E) and peak strength (σ_p).

t_{Ni} (μm)	f_{Ni}	ρ (Mg m^{-3})	E (MPa)	σ_p (MPa)
0	0	0.046 ± 0.001	7.71 ± 1.62	0.48 ± 0.01
15.1 ± 0.5	0.21 ± 0.01	0.138 ± 0.005	35.0 ± 4.4	2.86 ± 0.18
27.8 ± 1.8	0.33 ± 0.02	0.223 ± 0.015	54.9 ± 6.6	6.22 ± 0.94
31.8 ± 1.1	0.36 ± 0.01	0.250 ± 0.010	62.7 ± 1.2	7.87 ± 0.48
43.8 ± 2.3	0.45 ± 0.02	0.343 ± 0.021	104.4 ± 6.8	11.41 ± 0.56
56.7 ± 1.4	0.53 ± 0.01	0.440 ± 0.010	97.1 ± 2.2	17.05 ± 0.90

3. Results

Fig. 4 presents a typical stress–strain curve for the starting (as-received) rapid prototyped micro-truss. There is an initial elastic region having a modulus of $E = 7.71 \pm 1.62$ MPa. Load/unload profiles within this initial elastic region were found to overlap, similar to the results presented by Wallach and Gibson [24]. The initial elastic region was followed by a peak stress at a value of $\sigma_p = 0.48 \pm 0.01$ MPa, after which point the truss core eventually collapsed by strut fracture at a collapse strength of ~0.05 MPa. This rapid strength loss is similar to what has been reported for certain brittle polymer and ceramic foams (e.g. [25,26]). The stress increased again at a strain of ~0.6 as final densification of the core material occurred.

Fig. 5 presents typical stress–strain curves for the nanocrystalline Ni hybrid micro-trusses. Even for the thinnest nanocrystalline sleeves ($t_{Ni} = 15.1$ μm, corresponding to a strut area fraction of only $f_{Ni} = 0.21$), the elastic modulus had increased by ~350% and the peak strength by ~500%. For the thickest nominal coating ($t_{Ni} = 58.1$ μm), the compressive modulus was $E = 100$ MPa and the peak strength was $\sigma_p = 17.8$ MPa, values summarized in Table 1. In addition, the nanocrystalline sleeves had the effect of changing the strut failure mechanism to inelastic buckling. This can be seen in Fig. 6, which presents an SEM micrograph of a sample ($t_{Ni} = 45.2$ μm) loaded to a strain of ~0.25, i.e., to after the peak in the stress–strain curve. Although local wrinkling occurred at mid-strut, no cracks were seen within the failed compression members. This change in failure mechanism can also be seen from the post-peak region of the stress–strain curve. Unlike the case for the starting rapid prototyped core, the struts of the nanocrystalline Ni hybrid micro-truss were still able to support some load before final densification. The minimum collapse strength increased from 0.05 MPa ($0.1\sigma_p$) for the acrylic micro-truss to ~1 MPa ($0.4\sigma_p$) for the thinnest Ni sleeves and to ~8 MPa ($0.45\sigma_p$) for the thickest case.

Careful investigation of the nanocrystalline Ni micro-truss stress–strain curves indicated a series of nearly instantaneous load drops occurring after the peak buckling stress

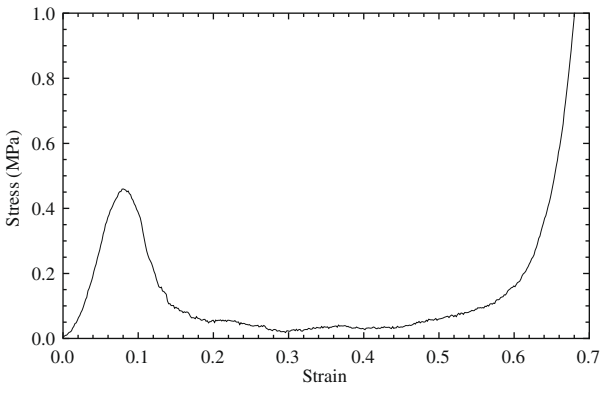

Fig. 4. Typical compressive stress–strain curve for the starting (as-received) polymer micro-truss.

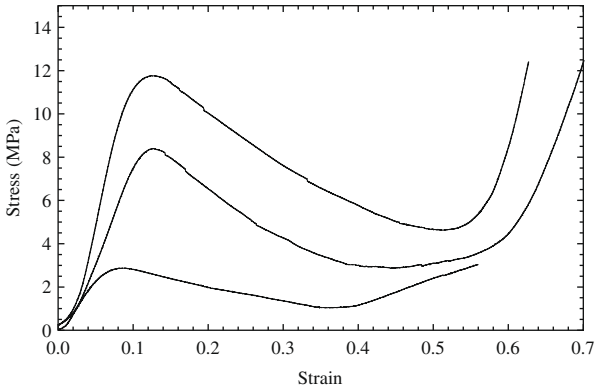

Fig. 5. Typical compressive stress–strain curves of nanocrystalline Ni micro-trusses; the curves shown have sleeve thicknesses of $t_{Ni} = 15.3$, 32.2 and 44.4 μm.

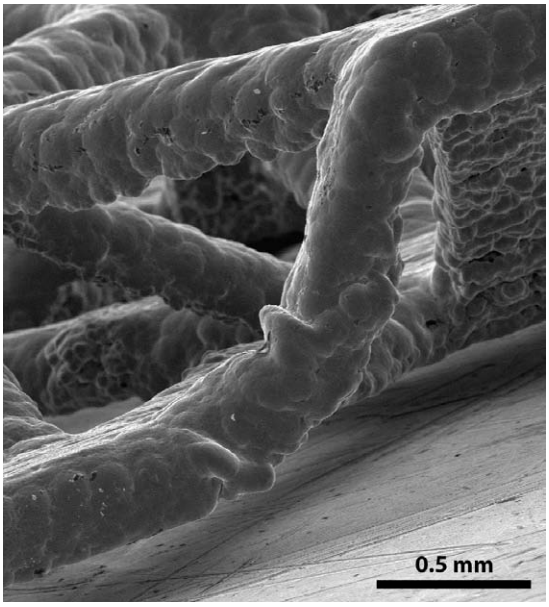

Fig. 6. SEM micrograph showing inelastic buckling failure of a nanocrystalline strut.

had been reached (Fig. 7a). These load drops could be seen more clearly by plotting the slope of the tangent to the stress–strain curve as a function of strain (Fig. 7b). SEM characterization of nanocrystalline Ni micro-trusses loaded within this regime showed that the tensile struts of the face-sheets progressively fractured after the pyramidal units of the core had buckled (Fig. 8). Periodic load drops were also seen in the uniaxial compression stress–strain curves of nanocrystalline Ni–Fe/aluminum micro-trusses [16]. However, the failure mechanisms associated with the load drops in the two cases are different. For the Ni–Fe/Al hybrid, the load drops began before the peak strength was reached; SEM characterization indicated that crack formation in the nanocrystalline Ni–Fe sleeves was associated with strut rotation prior to inelastic buckling [16]. In the present study, tensile failure of the face-sheet struts occurred after inelastic buckling collapse of the core struts. It should be

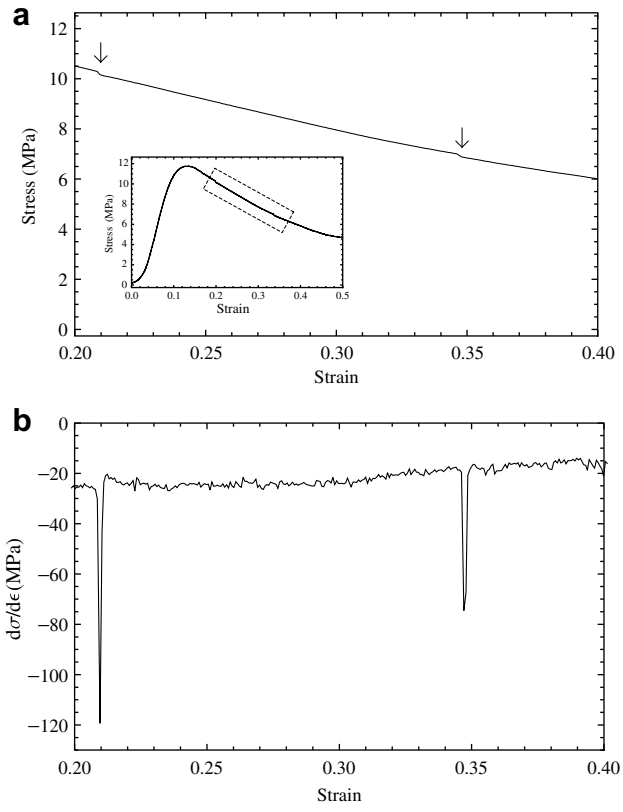

Fig. 7. Load drops (a) and slope of the tangent (b) for the stress–strain curve of a nanocrystalline Ni micro-truss ($t_{Ni} = 0.45$ μm).

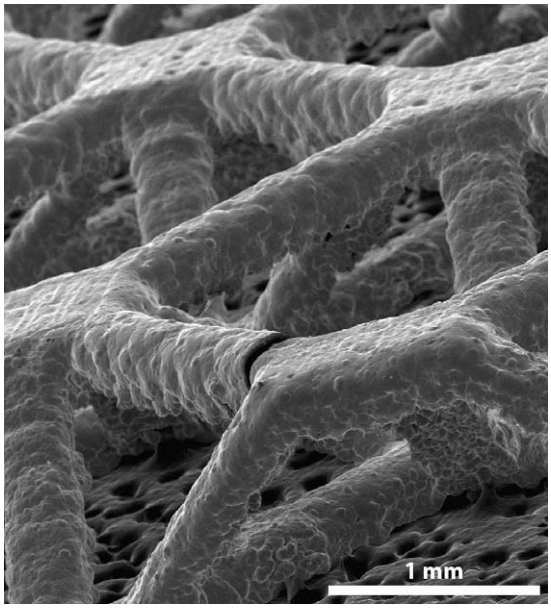

Fig. 8. SEM micrograph of a nanocrystalline Ni micro-truss showing tensile fracture of a face-sheet strut.

noted that while the peak strengths of the nanocrystalline Ni micro-trusses from the present study (2.7–17.8 MPa) are comparable to the peak strengths previously reported for the nanocrystalline Ni–Fe/Al hybrids (1.9–12.5 MPa

[16]), the corresponding densities of the present micro-trusses are approximately 30% lower.

4. Discussion

4.1. Elastic modulus

Models for the elastic modulus of periodic cellular micro-trusses generally overpredict the experimentally measured values (e.g. [27–31]). In the present study, a knockdown factor α was used to account for this compressive modulus overprediction. The compressive modulus, E, of a pyramidal micro-truss can then be expressed as (after [32])

$$E = \alpha E_S (V_{Ni} + V_{polymer}) \sin^4 \omega \quad (2)$$

where E_s is the elastic modulus of the individual struts, V_{Ni} and $V_{polymer}$ are the solid volume fractions of the Ni and polymer in the truss core (defined as the volume of the strut components in the truss core divided by the total volume of the truss core), and ω is the strut angle. Assuming uniform strain within the nickel and polymer, the effective modulus of the composite nickel–polymer strut, E_s, was estimated using a rule of mixtures approach (after [33])

$$E_S = f_{Ni} E_{Ni} + (1 - f_{Ni}) E_{polymer} \quad (3)$$

where f_{Ni} is the fractional Ni strut cross-sectional area (Table 1), and E_{Ni} and $E_{polymer}$ are the elastic moduli of the nanocrystalline Ni and acrylic photopolymer. Fig. 9 presents the measured elastic modulus values as a function of the nanocrystalline Ni sleeve thickness as well as the line of best fit (corresponding to $\alpha = 0.061$).

Significant overpredictions in the elastic modulus have been attributed to factors such as bedding-in of truss nodes, geometric imperfections and uneven loading during initial stages of loading (e.g. [27–31]). In particular, the idealized model assumes that all strain energy is transferred into the struts as axial deformation. However, since eccentricities will always exist in a real micro-truss, the truss members are likely undergoing a combination of axial and transverse loading. The model also does not account for edge effects or strain absorbed by the face-sheets, the latter of which results in transverse expansion of the truss. Preventing this expansion by confining the micro-truss laterally during compression (or producing a truss with rigid face-sheets) has been shown to increase the measured compressive modulus (e.g. [34,35]).

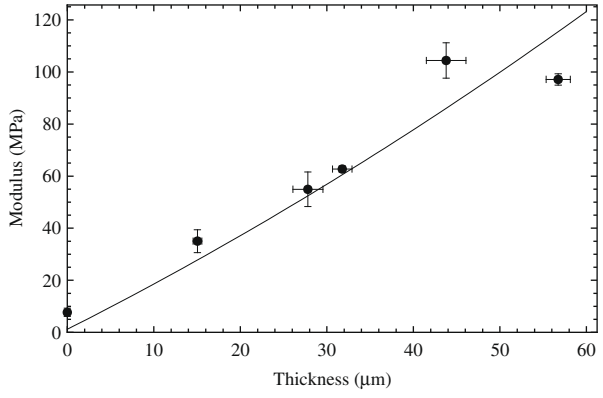

Fig. 9. Elastic modulus of the micro-trusses plotted as a function of the nanocrystalline Ni sleeve thickness. Also shown is a plot of Eq. (2) corresponding to the line of best fit ($\alpha = 0.061$).

4.2. Peak compressive stress

Similar to the case for elastic modulus, compressive strength models typically overpredict the peak strength of micro-truss materials (e.g. [27–31]), and a knockdown factor β was introduced in the present study. A force balance along the compression axis can be used to derive an equation relating the peak strength of the entire truss (σ_P) to the failure stress of the individual struts (σ_S) (after [32])

$$\sigma_P = \beta \sigma_S (V_{Ni} + V_{polymer}) \sin^2 \omega \quad (4)$$

If the struts are short and stocky they will fail either by yielding or by fracture, such that $\sigma_S = \sigma_F$, where σ_F is the failure strength of the strut material. If the struts are more slender, they will fail by buckling and σ_S is replaced by the critical buckling stress (after [33])

$$\sigma_{CR} = \frac{k^2 \pi^2 E_t I}{A l^2} \quad (5)$$

where E_t is the tangent modulus ($E_t = \partial\sigma/\partial\varepsilon$), k is a constant representing the end fixity condition, l is the strut length, A is the strut cross-sectional area and I is the moment of inertia for the section.

For the assumed elastic/perfectly plastic constitutive behaviour of the polymer core, failure will occur either by elastic buckling (i.e., $E_t = E$, the Young's modulus), for long and slender struts, or by yielding (i.e., $\sigma_F = \sigma_{YS}$), for short and stocky struts. Using the moment of inertia of the rectangular cross-section polymer struts ($I_{polymer} = 1.90 \times 10^{-4}\,mm^4$) and the modulus of the acrylic photopolymer, critical buckling stresses of 24 and 96 MPa are obtained for the limiting cases of pin joint ($k = 1$ (e.g. [24,27,35])) and rigid joint ($k = 2$ (e.g. [28,30])) fixity conditions, respectively. Note that the actual end constraints are likely to be intermediate to $k = 1$ and $k = 2$. The yield strength of the acrylic photopolymer (32 MPa) is at the low end of this critical buckling stress range, which is consistent with the experimental observation that initial strut failure was not reversible (elastic buckling).

Failure of the composite polymer/nanocrystalline Ni struts can be modeled after the inelastic buckling theory developed by Shanley [33]. Since the stiffness and yield strength of the polymer was much lower than that of the nickel, the polymer contribution to the buckling strength and load capacity was considered to be negligible. The moment of inertia for a hollow rectangular section of Ni with the same centroidal axis as the polymer section can be expressed as

$$I_{\mathrm{Ni}} = \frac{(b + 2t_{\mathrm{Ni}})(a + 2t_{\mathrm{Ni}})^3}{12} - I_{\mathrm{polymer}} \quad (6)$$

The critical stress in the nickel was determined by solving the equation

$$\sigma_{\mathrm{CR,Ni}} = \frac{k^2\pi^2 E_{\mathrm{t,Ni}} I_{\mathrm{Ni}}}{l^2 f_{\mathrm{Ni}}(a + 2t_{\mathrm{Ni}})(b + 2t_{\mathrm{Ni}})} \quad (7)$$

where $E_{\mathrm{t,Ni}}$ was determined using the polynomial fit to the reference tensile curve of electrodeposited nanocrystalline Ni. Fig. 10 presents the measured peak stress as a function of nanocrystalline Ni sleeve thickness. Also shown are the predicted peak stresses of the micro-trusses using pin joint ($k = 1$) end constraints for the ideal case ($\beta = 1$) and the line of best fit (corresponding to $\beta = 0.59$).

There are several issues that may be contributing to the knockdown factor in the inelastic buckling performance. First, struts that are not straight, uniform, or otherwise ideal will exhibit a reduction in the critical buckling stress (e.g. [33]). This may be especially significant for the micro-trusses of the present study that have strut cross-section dimensions close to the ~75 μm resolution limits of the rapid prototyper [17]. Since the electrodeposited nanocrystalline sleeve is conformal to the polymer pre-form, surface flaws from rapid prototyping will generally be reproduced in the electrodeposited sleeve (Fig. 2). In addition, residual stresses can form during the electrodeposition of nanocrystalline materials (e.g. [36]), which may also act to reduce the critical buckling strength.

4.3. Composite strut design

Micro-truss failure is controlled by a complex interaction of geometry and material properties. For example, while the polymer core is needed as a cathode support during electrodeposition, it also serves a structural function by distributing the nanocrystalline material away from the neutral bending axis of the struts. The larger the diameter of the polymer struts, the greater the structural efficiency of the nanocrystalline sleeve. At the same time, there is obviously a weight penalty to be paid for the polymer core. This can be seen in Fig. 11, which plots the specific elastic modulus (E/ρ) for nanocrystalline Ni/polymer core micro-trusses as a function of the polymer strut cross-sectional dimension (using a square strut cross-section and assuming a constant knockdown factor of $\alpha = 0.061$). The specific stiffnesses are plotted for mass densities of Ni ranging from 0.05 to 1 Mg m^{-3} (mass of electrodeposited Ni divided by the volume of the micro-truss). Because the specific stiffness of the Ni sleeve is greater than that of the polymer core, the overall micro-truss specific stiffness decreases with increasing polymer core dimension for a given mass density of electrodeposited Ni. On the other hand, there is an optimal polymer strut cross-section for maximizing the specific strength (σ_p/ρ) of the nanocrystalline Ni/polymer core micro-trusses, which can be seen in Fig. 12 (using $k = 1$ and a constant knockdown factor of $\beta = 0.59$). There is a small shift in the position of the peak specific strength with increasing electrodeposited Ni mass density; the peak occurs at a polymer core edge length of ~0.14 mm for a Ni mass density of 0.05 Mg m^{-3} and increases to ~0.2 mm for a mass density of 0.5 Mg m^{-3}. At higher mass

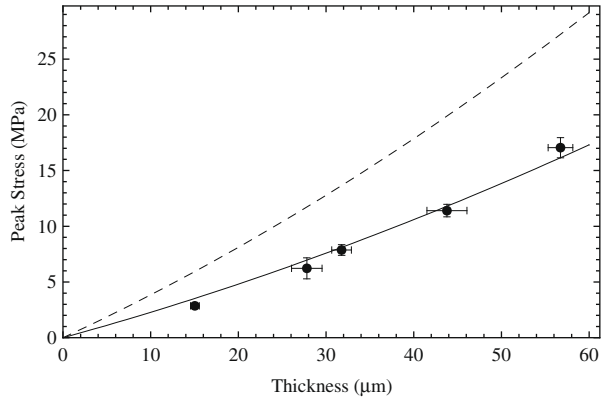

Fig. 10. Peak stress of the nanocrystalline Ni micro-trusses plotted as a function of the nanocrystalline Ni sleeve thickness. Also shown are the plots of Eq. (4) for an end constraint condition of $k = 1$ in the ideal case ($\beta = 1$, dashed line) and the line of best fit corresponding to $\beta = 0.59$ (solid line).

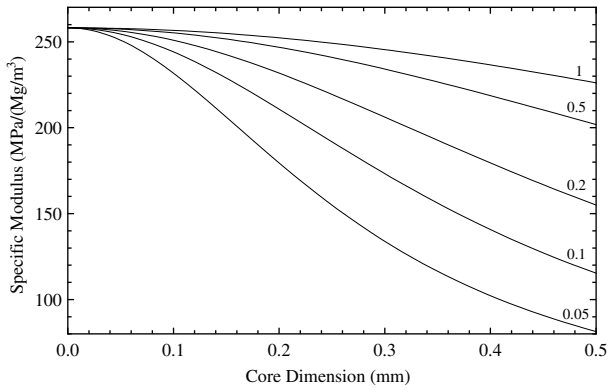

Fig. 11. Specific modulus plotted as a function of the square polymer cross-sectional core dimension for nanocrystalline Ni mass densities ranging from 0.05 to 1 Mg m^{-3}.

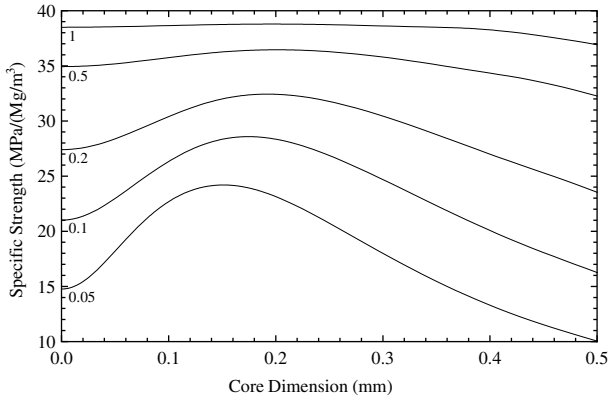

Fig. 12. Specific strength plotted as a function of the square polymer cross-sectional core dimension for nanocrystalline Ni mass densities ranging from 0.05 to 1 Mg m^{-3}.

densities of Ni, the core edge length plays a progressively smaller role in determining the peak specific strength.

The buckling strength of the nanocrystalline strut is proportional to the product of the Ni tangent modulus and the moment of inertia of the sleeve. The peak specific strength can be understood in terms of the trade-off between the gain in structural efficiency with increasing polymer core dimension and the reduction in tangent modulus at the critical buckling stress. During the initial specific strength increase, the improved sectional efficiency of the sleeve more than compensates for the added weight penalty of the polymer core. However, the tangent modulus at the critical buckling stress continuously decreases with increasing core dimension (Fig. 13), eventually offsetting the increased sectional efficiency. Therefore, when used in micro-truss form it is not just the strength of the nanocrystalline material that matters, but also the particular shape of the elastic to plastic transition in the knee of the stress–strain curve.

Fig. 14 plots the measured peak strength of the nanocrystalline Ni micro-trusses as a function of density and illustrates how incorporating a cellular architecture within the nanocrystalline material allows new regions of material property space to be accessed. Also shown are reported yield strengths for nanocrystalline Ni [6,7,38–40] and conventional polycrystalline Ni [23,41]. While grain size reduction to the nanometer scale provides an enormous strength increase, the actual material performance is nevertheless limited to a comparatively narrow band of material property space. For the case of strength-limited design, the $\sigma^{1/2}/\rho$ performance index of the nanocrystalline Ni micro-trusses (9.38–12.25 $MPa^{1/2}\,m^3\,Mg^{-1}$) is larger than that of the bulk nanocrystalline Ni (3.14 $MPa^{1/2}\,m^3\,Mg^{-1}$). Even better material performance indices for the micro-trusses could be obtained by strut optimization (e.g., Figs. 11 and 12). In addition, removing the polymer core after electrodeposition (by thermal decomposition or by chemical dissolution) would substantially enhance the weight specific performance. However, it should also be noted that removing the polymer core may promote new failure mechanisms, such as local wrinkling, which could affect the optimal strut design. Nanocrystalline micro-truss materials may be successful in applications that place a premium on specific strength and stiffness at low density. Advances in rapid prototyping and electrosynthesis methods can be expected to reduce the significance of the stiffness and strength knockdown factors. Finally, while a wide range of strut dimensions could be electroformed, the small-scale struts of the present study are amenable to applications including sandwich structures in MEMS components and in micro-air vehicle and micro-satellites [42,43].

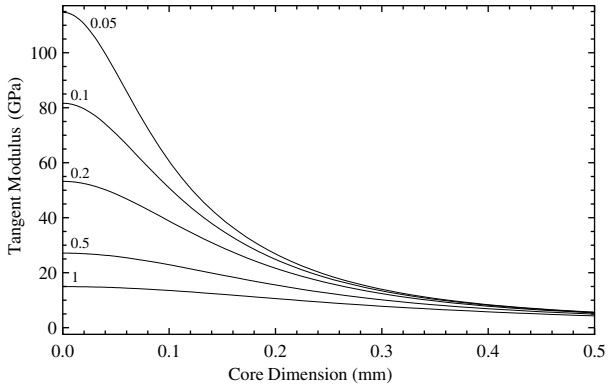

Fig. 13. Tangent modulus at the critical buckling stress plotted as a function of the square polymer cross-sectional core dimension for nanocrystalline Ni mass densities ranging from 0.05 to 1 Mg m^{-3}.

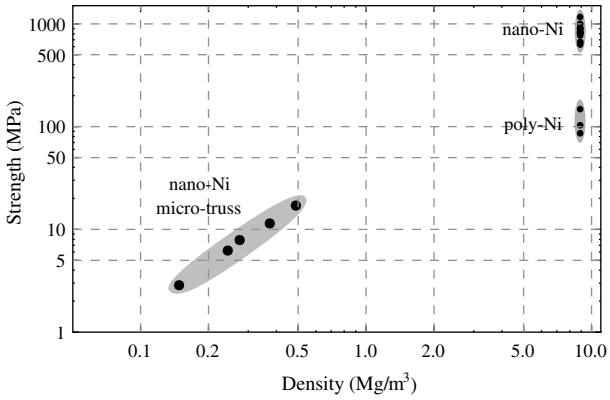

Fig. 14. Strength vs. density materials property map showing the measured peak strength of the nanocrystalline Ni micro-trusses and the reported yield strength values for nanocrystalline Ni [6,7,38–40] and conventional polycrystalline Ni [23,41].

5. Conclusions

Nanocrystalline materials can access new regions of material property space by incorporating an internal periodic cellular architecture. In the present study, high-strength nanocrystalline sleeves were electroformed around a rapid prototyped micro-truss polymer; the overall density of the hybrid micro-trusses was ~1.5–5% of bulk nanocrystalline Ni. Failure in uniaxial compression occurred by inelastic buckling of the core members and tensile fracture of the face-sheet members. Even the thinnest nanocrystalline sleeve thicknesses of ~15 μm resulted in a ~350% increase in elastic modulus and a ~500% increase in peak strength over that of the starting polymer core. In part, this is because the polymer serves to distribute the nanocrystalline material away from the neutral bending axis of the micro-truss struts. Experimental knockdown factors were determined from the idealized models for strength and modulus, providing a starting point for developing the mechanical properties of nanocrystalline micro-truss materials.

Acknowledgement

Financial support from the Natural Sciences and Engineering Research Council of Canada (NSERC) is gratefully acknowledged.

References

[1] Gleiter H. Prog Mater Sci 1989;33:223.
[2] Gleiter H. Acta Mater 2000;48:1.
[3] Kumar KS, Van Swygenhoven H, Suresh S. Acta Mater 2003;51:5743.
[4] Meyers MA, Mishra A, Benson DJ. Prog Mater Sci 2006;51:427.
[5] Koch CC. J Mater Sci 2007;42:1403.
[6] Wang N, Wang Z, Aust KT, Erb U. Mater Sci Eng A 1997;237:150.
[7] Zimmerman AF, Palumbo G, Aust KT, Erb U. Mater Sci Eng A 2002;328:137.
[8] Dalla Torre F, Van Swygenhoven H, Victoria M. Acta Mater 2002;50:3957.
[9] Fan GJ, Fu LF, Qiao DC, Choo H, Liaw PK, Browning ND. Scripta Mater 2006;54:2137.
[10] Brooks I, Lin P, Palumbo G, Hibbard GD, Erb U. Mater Sci Eng A 2008;491:412.
[11] Palumbo G, Gonzalez F, Tomantschger K, Erb U, Aust KT. Plat Surf Fin 2003;90:36.
[12] Wei HS, Hibbard GD, Palumbo G, Erb U. Scripta Mater 2007;57:996.
[13] Ashby MF. Materials selection in mechanical design. 3rd ed. Oxford: Butterworth-Heinemann; 2005.
[14] Ashby MF, Evans AG, Fleck NA, Gibson LJ, Hutchinson JW, Wadley HNG. Metal foams a design guide. Oxford: Butterworth-Heinemann; 1999.
[15] Ashby MF. Philos Trans Royal Soc A 2006;364:15.
[16] Suralvo M, Bouwhuis B, McCrea JL, Palumbo G, Hibbard GD. Scripta Mater 2008;58:247.
[17] FineLine Prototyping, http://www.finelineprototyping.com.
[18] Erb U, El-Sherik AM. US Patent 5,353,266; October 1994.
[19] Erb U, El-Sherik AM, Cheung CKS, Aus MJ. US Patent 5,433,797; July 1995.
[20] El-Sherik AM, Erb U, Palumbo G, Aust KT. Scripta Mater 1992;27:1185.
[21] El-Sherik AM, Erb U. J Mater Sci 1995;30:5743.
[22] Integran Technologies Inc., unpublished research.
[23] Mankins WL, Lamb S. Nickel and nickel alloys. In: Lampman SR, Zorc TB, editors. ASM handbook. Properties and selection: nonferrous alloys and special-purpose materials, vol. 2. Materials Park, OH: ASM International; 1990. p. 37.
[24] Wallach JC, Gibson LJ. Int J Solids Struct 2001;38:7181.
[25] Song B, Chen W, Frew DJ. J Compos Mater 2004;38:915.
[26] Costa Oliveira FA, Dias S, Vaz MF, Fernandes JC. Mater Sci Forum 2004;455–456:172.
[27] Deshpande VS, Fleck NA, Ashby MF. J Mech Phys Solids 2001;49:1747.
[28] Kooistra GW, Deshpande VS, Wadley HNG. Acta Mater 2004;52:4229.
[29] Wadley HNG. Philos Trans Royal Soc A 2006;364:31.
[30] Kooistra GW, Wadley HNG. Mater Des 2007;28:507.
[31] Moongkhamklang P, Elzey DM, Wadley HNG. Compos A 2008;39:176.
[32] Deshpande VS, Fleck NA. Int J Solids Struct 2001;38:6275.
[33] Shanley FR. Strength of materials. New York: McGraw-Hill; 1957.
[34] Bouwhuis BA, Hibbard GD. Metall Mater Trans B 2006;37:919.
[35] Lim J-H, Kang K-J. Int J Solids Struct 2006;43:5228.
[36] El-Sherik AM, Shirokoff J, Erb U. J Alloys Compd 2005;389:140.
[38] Ebrahimi F, Bourne GR, Kelly MS, Matthews TE. Nanostruct Mater 1999;11:343.
[39] Ebrahimi F, Ahmed Z, Morgan KL. Mater Res Soc Symp Proc 2001;634:B271.
[40] Gu D, Lian J, Jiang Z, Jiang Q. Scripta Mater 2006;54:579.
[41] Thompson AW. Acta Metall 1977;25:83.
[42] Brittain ST, Sugimura Y, Schueller OJA, Evans AG, Whitesides GM. J MEMS 2001;10:113.
[43] Stampfl J, Fouad H, Seidler S, Liska R, Schwager F, Woesz A, et al. Int J Mater Prod Technol 2004;21:28.